

# The globular cluster NGC 6642: Evidence for a depleted mass function in a very old cluster

E. Balbinot<sup>1</sup>, B.X. Santiago<sup>1</sup>, E. Bica<sup>1</sup> and C. Bonatto<sup>1</sup>

<sup>1</sup>*Departamento de Astronomia, Universidade Federal do Rio Grande do Sul, Av. Bento Gonçalves 9500  
Porto Alegre 91501-970, RS, Brazil*

21 November 2021

## ABSTRACT

We present photometry for the globular cluster NGC 6642 using the F606W and F814W filters with the ACS/WFC third generation camera on board of Hubble Space Telescope. The Colour Magnitude Diagram shows sources reaching  $\approx 6$  *mags* below the turn-off in  $m_{F606W}$ . A theoretical isochrone fitting was performed and evolutionary parameters were obtained, such as the metallicity  $[Fe/H] = -1.80 \pm 0.2$  and age  $\log(\tau(\text{yrs})) = 10.14 \pm 0.05$ . We confirm that NGC 6642 is located in the Galactic bulge, with a distance to the Sun  $d_{\odot} = 8.05 \pm 0.66$  *kpc* and the reddening  $E(B - V) = 0.46 \pm 0.02$ . These values are in general agreement with those of previous authors. About 30 blue stragglers were found within the central 1.6 pc of NGC 6642. They are strongly concentrated to the very central regions. The cluster displays a well-developed horizontal branch, with a much redder morphology than that of typical old halo globular clusters of similar metallicity. Completeness corrected luminosity and mass functions were obtained for different annuli centred on NGC 6642. Their spatial variation indicates the existence of mass segregation and depletion of low mass stars. Most striking is the inverted shape of the mass function itself, with an increase in number as a function of increasing mass. This has been previously observed in other globular clusters and is also the result of N-body simulations of stellar systems which have undergone  $\simeq 90\%$  of their lifetime and which are subjected to strong tidal effects. We also analysed the density profile and concluded that NGC 6642 has a collapsed core, provided completeness effects are correctly accounted for. We thus conclude from independent means that NGC 6642 is a very old, highly-evolved, core-collapsed globular cluster with an atypical HB morphology. Its current location close to perigalactic, at only 1.4 *kpc* from the Galactic centre, may contribute to this high level of dynamical evolution and stellar depletion.

**Key words:** (*Galaxy:*) globular clusters: general; (*Galaxy:*) globular cluster: individual: NGC6642; Galaxy: structure

## 1 INTRODUCTION

Given their relatively high contrast with the background, the census of globular clusters (GCs) in the Galaxy is near completion. The dense and highly extincted Galactic bulge, specially its inner regions, is the site where most missing clusters, perhaps 10% of the total known population, are expected to be (Ivanov et al. 2005, Ortolani et al. 2006 and references therein). The bulge is known to host old but fairly metal-rich stellar populations, with high  $[\alpha/Fe]$  ratios, indicating that it formed on a short time-scale early in the Galactic history (Origlia et al. 2005). The bulge is thus an appropriate region to look for ancient GCs with distinct metallicities from those in the outer stellar halo. The bulge

environment may also cause extreme dynamical evolution of star clusters due to bulge shocking and strong tidal effects (Aguilar et al. 1988; Shin et al. 2008). For old enough GCs, effects of close stellar encounters, which lead to mass segregation and stellar evaporation, are certain to be found in them as well (Baumgardt & Makino 2003).

Analyses of the structure and dynamical evolution of bulge GCs require high-resolution imaging in order to resolve individual stars in their cores and to effectively subtract contaminating field stars. The Advanced Camera for Surveys in the Wide Field Channel (ACS/WFC) on board of the Hubble Space Telescope (HST) has provided a significant leap in the amount of such data on GCs, not only in the bulge, but also elsewhere (Sarajedini et al.

2007; Richer et al. 2008; Paust et al. 2009). Recently, Marin-Franch et al. (2008) provided ACS photometry for 64 halo GCs and derived relative ages. The ACS allows to study extremely dense fields using point source photometry. With such technique it is feasible to use stellar interior models to obtain evolutionary parameters of the cluster stellar population.

NGC 6642 (also designated by ESO 522-SC32 and GCl-97) is located at  $l = 9.81^\circ$ ,  $b = -6.44^\circ$ , therefore projected towards the Galactic bulge. It is thus superimposed onto bulge and inner halo stellar populations. Dynamical studies of this GC, as well as other bulge clusters, have thus been extremely difficult, due to limitations of ground based images. Structural parameters were found by Trager et al. (1995), such as core radius  $r_{\text{core}} = 6.1''$ , concentration parameter  $c = 1.99$  and half light radius  $r_h = 44''$ . They also conclude that NGC 6642 is a core-collapsed candidate. Using spectroscopy of individual stars, Minniti (1995) derived  $[Fe/H] = -1.40$ . Later Barbuy et al. (2006) using BVI photometry with SOAR, found  $[Fe/H] = -1.3$ , reddening  $E(B - V) = 0.42 \pm 0.03$  and  $d_\odot = 7.2 \text{Kpc}$  ( $(m - M)_0 = 14.3$ ). In the catalogue compiled by Harris (1996), similar results are quoted:  $(m - M)_V = 15.90$ ,  $E(B - V) = 0.41$  and  $[Fe/H] = -1.35$ . All these results are from ground-based studies. The only space-based dataset on NGC 6642 so far is that from the compilation of Colour-Magnitude Diagrams (CMDs) from Piotto et al. (2002), who used the Wide Field Planetary Camera (WFPC2) snapshots.

In this work we present F606W (Broad V) and F814W (Broad I) ACS photometry of NGC 6642. Notice that NGC 6642 is not included in the sample by Marin-Franch et al. (2008) since it is projected towards the bulge. We use this photometry not only to derive metallicity, reddening, distance and age, but also to make a detailed analysis of its e.g. structure, including radial density profile (RDP), luminosity and mass functions, horizontal branch (HB) morphology and blue stragglers. This paper is organised in the following way: in Sect. 2 we describe the data and the reduction process. In Sect. 3 we present the data analysis. In Sect. 4 there is a brief discussion on the cluster age and evolution; we also present the concluding remarks.

## 2 DATA

The images were retrieved from the Space Telescope Science Institute<sup>1</sup> (STScI) data archive and were automatically reduced by the STScI pipeline, i.e. they were corrected for bias, dark current and were divided by the flatfield image. The images of NGC 6642 are part of the proposal 9799 and were obtained in 2004. They cover a  $202'' \times 202''$  field of view at a spatial scale of  $0.049''/\text{pixel}$ , with a gap between the CCDs. Two exposures were taken in the F606W and F814W filters: short (10s) and long (340s). In Fig. 1 we show the F814W short exposure for the cluster's central region. Notice the detached bright central object composed by unresolved individual stars located near the cluster centre.

The photometry was carried out using the DOLPHOT software (Dolphin et al. 2000). The following steps were taken

to prepare the images for photometry: (i) the task ACSMASK masks all bad pixels, (ii) the task SPLITGROUPS splits the multi-extension FITS image into single chip images. As described in the DOLPHOT manual, a position reference image must be adopted, preferentially a deep and uncrowded one. We used the F814W long exposure with geometric corrections applied (drizzled image) as the reference frame. The photometric measurements were performed on the calibrated frames, not corrected for geometric distortions. We adopted the recommended parameters in the DOLPHOT manual. The output magnitudes, in the VEGAMAG system, were corrected for aperture and charge transfer efficiency (CTE). The output position of each star is subsequently corrected for geometrical distortion using the reference frame.

In order to have a high quality CMD of NGC 6642, the output parameters of DOLPHOT were used to filter out non-stellar objects, cosmic rays and other spurious detections such as wings and diffraction rings. Basically the *sharpness* parameter measures if the source is too sharp (positive values) or extended (negative values). The *crowding* parameter measures how much the light of a star is due to close neighbours used in the PSF fit. As recommended in DOLPHOT, no  $\chi^2$  cut has been applied as a star selection criterion, due to its dependence on brightness. The following cuts were used:  $-0.1 \leq \text{sharpness} \leq 0.1$ ;  $\text{crowding} \leq 0.6$ ;  $\text{roundness} \leq 0.35$ . Only stars with type 1 and error type less than 8 in the DOLPHOT classification system were kept. The total number of stars found with accurate photometry in both passbands is  $\sim 32000$ .

A sanity check was performed to verify the quality of our photometry. We applied the bandpass transformation given by Sirianni et al. (2005) to convert the observed HB and main-sequence turn-off (MSTO) magnitudes and colours from F606W and F814W to Johnson V and I. They were then compared to the CMD from Barbuy et al. (2006). We have  $V_{HB} = 16.40 \pm 0.03$  as the mean HB V band magnitude and associated error, whereas Barbuy et al. (2006) got  $V_{HB} = 16.35 \pm 0.04$ . As for the MSTO, our CMD yields  $(V, V - I) = (19.75, 0.94)$ , compared to  $(V, V - I) = (19.7, 0.95)$  from those authors. We thus conclude that both photometries agree within the uncertainties.

DOLPHOT was employed again, this time in the artificial-star mode. Using fake-star experiments, we determined completeness as a function of magnitude, colour and position in the cluster,  $c(m_{F606W}, m_{F606W} - m_{F814W}, R)$ . The task ACSFAKELIST was used to generate artificial stars together with a Perl script. They were generated within the ranges  $20 \leq m_{F606W} \leq 27$  mag and  $0 \leq (m_{F606W} - m_{F814W}) \leq 2.5$ . We adopted bin sizes of 1 mag in  $m_{F606W}$ , 0.5 mag in  $(m_{F606W} - m_{F814W})$  and 100 pixels in distance from the cluster centre. The number of stars generated in a single realization of the experiment was never larger than 10% of the total original number in each region of the image. To build statistics, we performed 3 experiments for each  $(m_{F606W}, m_{F606W} - m_{F814W}, R)$  bin. A total of  $\sim 1.2 \times 10^5$  stars were generated. The images with artificial stars added underwent the same photometric and classification process as the original ones. As usual,  $c$  was taken as the ratio between the number of recovered artificial stars to the total. The result of the completeness analysis on the CMD plane is shown in Fig. 2, where we sum the results over all the radii. There is a strong colour dependence in the expected

<sup>1</sup> <http://www.stsci.edu/>

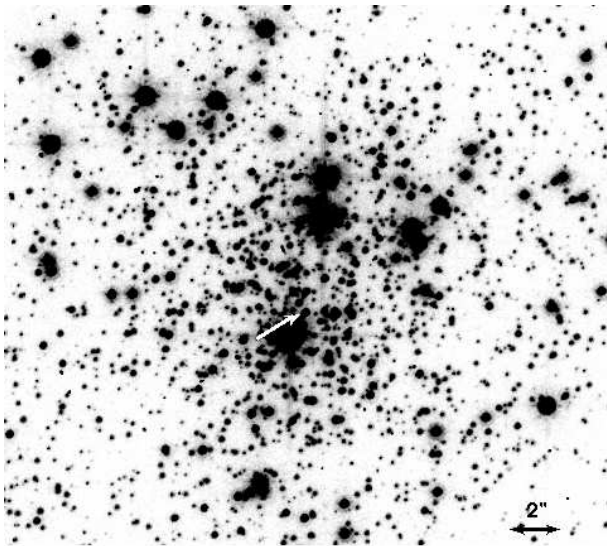


**Figure 1.** NGC6642: Central region ( $22'' \times 21''$ ) of the F814W short exposure. North is up and East is right. The adopted centre is indicated by the white arrow. Notice the dense object, apparently formed by a clump of crowded stars just below the centre of this image. Even with ACS/HST the stars in the centre of NGC 6642 are not easily resolvable.

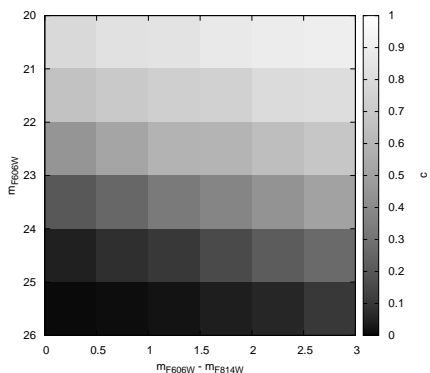


**Figure 2.** The position integrated completeness,  $c(m_{F606W}, m_{F606W} - m_{F814W})$  plotted over the CMD plane. The colour dependence is clear.

sense: at a fixed  $m_{F606W}$ , redder stars have higher  $c$  values, since they are brighter (and therefore more easily detected) in  $m_{F814W}$ .

### 3 ANALYSIS

#### 3.1 Colour-Magnitude Diagram

Fig. 3 shows the CMD for the stars located within  $r \leq 40''$  ( $\leq 1.6$  pc) from the nominal centre of NGC 6642. By restricting the image region, we strongly reduce field contamination. The selected central region contains about 40% of the total number of stars and only 10% of the field area. Therefore the vast majority of the stars in this field are expected to be GC members and should trace the evolutionary sequences of this object. In fact, we can see a well defined structure in the main sequence (MS) spanning  $\approx 6$  mag below the MSTO (located at  $m_{F606W} \simeq 19.2$ ). The sub-giant,

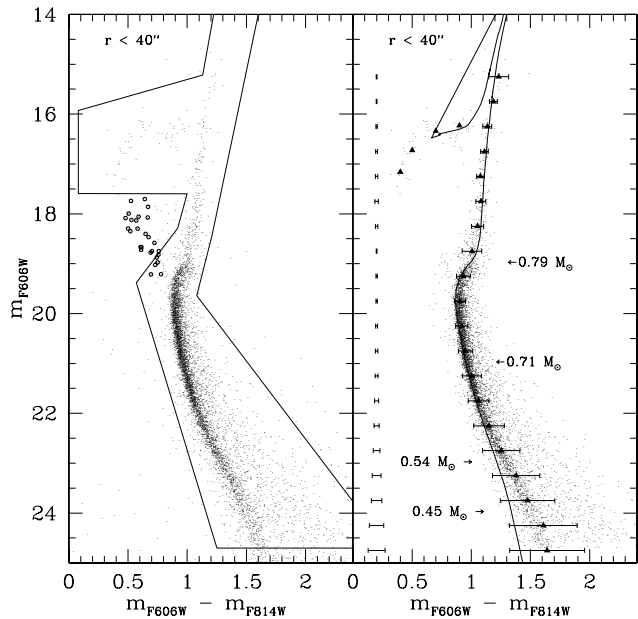


**Figure 3.** Left panel: CMD of all sources that satisfy the DOLPHOT parameter cuts and which are located within  $r \leq 40''$  from the centre of NGC 6642. We also show the region used to select the cluster evolutionary sequences. The BS candidates are marked with open circles. Right panel: same CMD as in the previous panel but cut according to the selected region. The solid triangles show the CMD fiducial line and corresponding dispersion. The mean photometric error is shown in the extreme left of this panel. Some mass values are given along the MS. The best-fit isochrone is over plotted and has the following parameters:  $\log(\text{age}) = 10.14$  ( $\tau = 13.8$  Gyrs);  $[Fe/H] = -1.80$ ;  $E(B - V) = 0.46$ ;  $(m - M)_0 = 14.55$ ;

red giant and horizontal branches (SGB, RGB and HB, respectively) are also clearly seen. Some candidate Asymptotic Giant Branch (AGB) stars are also present. The top of the RGB and AGB is not well sampled due to saturation, even in the short exposures. The solid contour on the left panel indicates our selected limits for these stellar evolutionary loci. The chosen limits also avoid effects of saturation and incompleteness. For instance, our cut-off at  $m_{F606W} \simeq 24.7$  at the CMD bottom avoids stars with completeness corrections  $1/c > 3$ . The open circles in the left panel indicate blue straggler (BS) candidates.

On the right panel of Fig. 3 the GC fiducial line is shown on top of the selected stars. The mean colour was calculated in magnitude bins for the MS, SGB and RGB. In the HB, the fiducial sequence was built by computing the mean magnitude in colour bins. The sequence is shown as solid triangles. We also show the dispersion around the fiducial points plus the mean photometric error for each magnitude bin. The photometric errors decrease with brighter magnitudes as expected up to  $m_{F606W} \simeq 19$ . At yet brighter magnitudes, the uncertainties initially increase because the measurements come from the short ACS exposures, since the long ones saturate at these bright levels. The dispersion around the fiducial points is slightly larger than the associated photometric errors. This is mostly due to the fact that the mean photometric errors are calculated over the entire image, while

the SGB and RGB stars are mainly located in the central region ( $r \leq 40''$ ) of the cluster, where crowding effects are not negligible. At the lower MS, unresolved binarism play a role in causing additional spread in colours. The dispersion of the fiducial line is larger near the bright end of the MSTO due to field stars and BS contamination. The NGC 6642 inner field CMD is used to visually fit isochrones. We use the isochrone grid computed<sup>2</sup> by Girardi et al. (2000) for that purpose. We also allow for variations in  $E(B - V)$  and  $(m - M)_0$  in the fits. The best-fit isochrone is shown on the right panel of Fig. 3. The corresponding parameters are  $\log(\tau(\text{yrs})) = 10.14$  and  $[Fe/H] = -1.80$ ,  $E(B - V) = 0.46$  and  $(m - M)_0 = 14.55$ .

The best-fit model describes most of the MS, including the MSTO, plus the SGB and RGB regions. A discrepancy is seen for  $m_{F606W} > 23$ , in the sense that the best-fit isochrone is too blue. This is likely the result of unaccounted opacity in the low-mass Padova models (Baraffe et al. 1998). The model HB is too short compared to the data, probably reflecting the model uncertainties at this evolutionary stage. The best fit we find is a compromise between the two discrepancies just mentioned. For instance, in order to fit the cluster lower MS, a lower age must be used, but this eliminates the HB in the model, as we just mentioned. On the other hand, to better fit the HB, a very low metallicity must be adopted, which jeopardizes the fits to the other loci and also is in clear conflict with the spectroscopic metallicity determination by Minniti (1995).

In order to determine parameter uncertainties and to test our visual fit, we generated model cluster fiducial lines and compared them with the observed one, shown in the right panel of Fig. 3. The models incorporated the effect of unresolved binaries, assuming a typical mass ratio of  $m_2/m_1 = 0.5$  and binary fraction of 50%. A  $\chi^2$ -like statistic was adopted in search of the best model and the parameter uncertainties were taken as the parameter range that satisfy the criterion  $\chi_{min}^2 \leq \chi^2 \leq 2 \times \chi_{min}^2$ . This approach led to the following results:  $\log(\tau(\text{yrs})) = 10.14 \pm 0.05$  and  $[Fe/H] = -1.80 \pm 0.2$ ,  $E(B - V) = 0.46 \pm 0.02$  and  $(m - M)_0 = 14.53 \pm 0.18$ . We thus confirm the parameters of NGC 6642 using two different methods.

### 3.2 Alternative age estimate

In this section we explore an alternative way to constrain the age of NGC 6642. A consistency check on the estimated age is obtained from the magnitude difference between the HB and the MSTO,  $\Delta V_{HB}^{TO}$ . We here adopt the same parametrization of this quantity as a function of  $[Fe/H]$  and  $\tau$  as used in Glatt et al (2008), which originally comes from Walker (1992):

$$\log \tau(\text{yrs}) = -0.045 [Fe/H] + 0.37 \Delta V_{HB}^{TO} - 0.24 \quad (1)$$

We estimate the HB and MSTO magnitudes as  $V_{HB} \simeq 16.25$  and  $V_{TO} \simeq 19.75$ , respectively. Notice that the HB in special has a considerable scatter around the quoted value. Assuming these values, we obtain  $\Delta V_{HB}^{TO} = 3.5$ , yielding in turn an age  $\tau = 13.7$  Gyrs. This estimate is consistent with that resulting from isochrone fitting.

### 3.3 Density Profiles

To analyse the density structure of NGC 6642, we computed the Radial Density Profile (RDP). Stars at various radii are weighted by the inverse of their completeness and their projected spatial density is obtained. The annuli used for the RDP construction were the same as in the completeness analysis.

Building a meaningful RDP, however, requires some cautionary steps. One is finding out the cluster centre, which is determined by the following method: (i) we count stars along the x-axis; (ii) the peak of this distribution is then assumed to be the x coordinate of the centre. The same procedure is then applied to the y-axis. For a spherical distribution this procedure clearly yields the centre of the distribution of stars, which may also be assumed to be approximately the centre of mass. Adoption of alternative methods show that our centre determination is robust.

Another important issue is the effect of field boundaries. They cause areal completeness effects at the outer radial bins, which had to be taken into account in the density estimates. For that purpose, we applied a Monte Carlo integral to find out the fraction of the total area in each bin which was effectively sampled by the image. Notice that in the proximity of the image boundary the error associated to the density estimate grows significantly due to the increased loss of areal sampling.

At each radius, the density of stars was given by:

$$\sigma(r) = \frac{\sum_i 1/c_i}{A(r)} \quad (2)$$

where the sum above takes place over all stars located within the annulus of radius  $r$ , whose effective area (corrected for image boundary) is  $A(r)$ . Each star is weighted by the inverse of its associated completeness  $c$  value, as estimated according to the procedure described in Sect. 2.

The resulting RDP is given as the solid circles in Fig. 4. The horizontal bars correspond to the radial bin size. The solid line is the best-fit King profile (see below). The  $1\sigma$  uncertainty range is also shown, as the grey region. In the inset we show the RDP that results from counting all stars with the same weight (therefore not corrected for completeness). Clearly, completeness corrections are crucial, especially in the central and denser regions, making the RDP much steeper than the uncorrected one. The completeness corrected RDP has no evidence for a core-like flattening. A fit to a King-like profile yields  $r_{core} = 8.6''$  and  $\sigma(0) = 9.4 \pm 0.7$  stars  $''^{-2}$ . The best-fit central density, however, is substantially lower than the observed one. Changing the density of field stars in the fit does not alter this conclusion. We thus conclude that NGC 6642 is in fact a core-collapsed GC.

Using the inner field CMD shown in Fig. 3 we can visually identify some BS. The number of candidate BS stars, as selected from their CMD position, is 50% higher in the GC region than in the general field. As the GC region represents only 10% of the total image, the excess of BS candidates per unit area is a factor  $\simeq 15$  higher than the field. This unequivocally shows that these stars have a high probability of being cluster members.

BS are known to be strongly concentrated towards the centre in most GCs, adding support to their possible origin from mergers of cluster stars or coalescence of tightly

<sup>2</sup> <http://stev.oapd.inaf.it/cgi-bin/cmd>

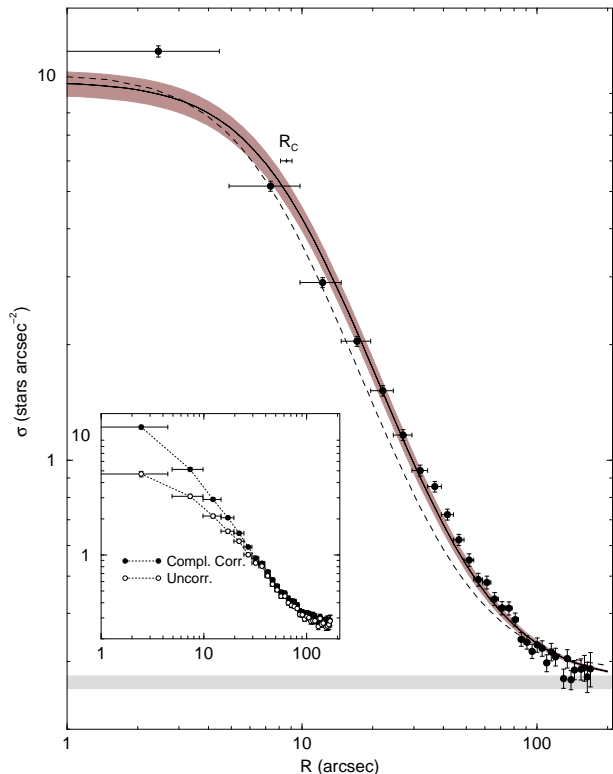


**Figure 4.** The RDP of NGC 6642 . We include only stars with  $m_{F606W} \leq 24$ . The filled circles show the completeness corrected number density profile, as given by eq. 2. The horizontal bars show the radial range of each bin. A King-like profile fit is shown as the solid line. The grey region is bracketed by the profiles resulting from varying the best-fit parameters by  $\pm 1\sigma$ . The dashed line is the best-fit profile assuming a higher value for the background star number density. The inset compares the completeness corrected profile (solid points) with the uncorrected profile (open symbols).

bound binaries. For the spatial study of the BS candidates we adopted the HB population as a comparison set. By doing so we eliminate the dynamical effects over the spatial distribution of stars since HB stars have a mass similar ( $m_{HB} \simeq 0.80 M_{\odot}$ ) to the mass of the turn-off stars.

In Fig. 5 we show the density distribution of BS and HB stars as a function of distance from the GC centre. The BS stars are in fact strongly concentrated towards the inner region of NGC 6642. This highly concentrated BS distribution is the rule in GCs, with the possible exceptions of NGC 2419 and  $\omega$  Cen (Dalessandro et al. 2008a; Ferraro et al. 2006). These latter two, however, are atypical as GCs in many aspects, showing evidence for a complex star formation history and very large unrelaxed cores (Norris et al. 1996; Sollima et al. 2005; Bellazzini 2007). The distribution in Fig. 5 also shows a region entirely depleted of BS candidates ( $15'' < R < 20''$ ) followed by a residual population further out. This is consistent with what has been observed in most GCs as discussed by Dalessandro et al. (2008b).

### 3.4 Luminosity and Mass Functions

In this section we study the distribution of stars as a function of luminosity and mass. These are important tools to

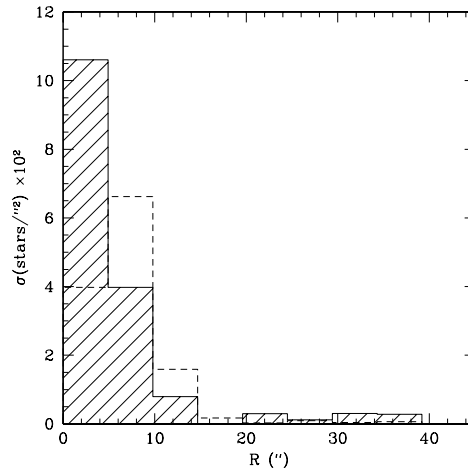


**Figure 5.** The density profile of selected BS (solid histogram) and HB (dashed histogram) stars, showing that most of the BS are located in the inner region of NGC 6642 . The BS population is more peaked than that of the HB stars.

assess dynamical effects, such as mass segregation and stellar evaporation, that take place throughout the GC lifetime.

The luminosity function (LF) is computed in the same radial bins as in the previous section. As in the case of RDPs, the LF is obtained by summing over stars in a given annulus, but this time also as a function of absolute magnitude  $M_{F606W}$ , as follows:

$$\phi(M_{F606W}) = \frac{dN}{dM_{F606W}} = \frac{\sum_i 1/c_i}{\Delta M_{F606W}} \quad (3)$$

The sum above is carried out over all stars in the annulus whose absolute magnitudes are within the bin around  $M_{F606W}$  with width  $\Delta M_{F606W}$ . The  $M_{F606W}$  values were computed by using the reddening and  $(m - M)_0$  derived in Sect. 3.1. Notice that we again weight stars according to the completeness function.

Fig. 6 shows the resulting LFs at different radial annuli.  $\Delta M_{F606W} = 0.5$  as adopted as bin size. A constant offset was added to the curves to avoid cluttering. Poisson error bars are also shown. The LFs extend towards fainter magnitudes at large radii because the completeness levels are higher at these lower density regions. Fig. 6 includes evolved stars as well as MS ones. The most striking variation in the LF shapes occurs in the MS domain ( $M_{F606W} > 3.5$ ), where the LF is clearly depleted of low luminosity stars and has a clear peak in the inner cluster regions. In contrast, the outer regions display flatter LFs all the way to the detection limit.

An alternative way to look for mass segregation is to compute the present day mass function (PDMF) from the observed LF. We use the best-fit Padova isochrone to convert stellar luminosities into initial masses. Only stars below  $m \simeq 0.8 M_{\odot}$  are considered in this conversion, since according to the model, mass loss is more pronounced at higher masses, signalling evolutionary stages later than the MS. We then bin stars as a function of initial mass. The resulting PDMFs are shown, again for the different radial annuli, in Fig. 7. A constant offset was again added for clarity. The star counts are normalized to unit solar mass intervals. Mass segregation now stands out more clearly, as the PDMF is

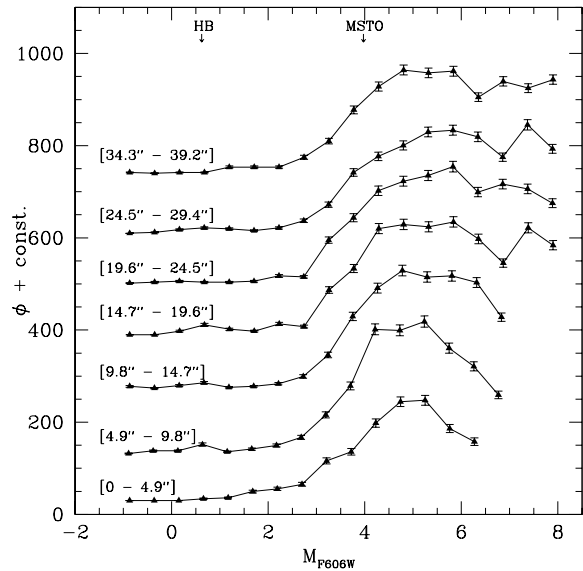


**Figure 6.** The LF of NGC 6642 stars at different radii, as indicated next to each curve. The positions of the MSTO and HB are indicated on the top. An offset was added to each curve to avoid overlap among them. In the inner regions, the completeness function falls off more rapidly as a function of magnitude, yielding a brighter cut-off limit.

systematically steeper in the central regions of NGC 6642. More striking, however, is the fact that the number of stars decreases towards lower masses, in contrast to most observed PDMFs. Assuming a Initial Mass Function (IMF) with a power-law behaviour,  $\xi \propto m^\alpha$  ( $\alpha = -2.35$  for a Salpeter IMF), the observed PDMF in NGC 6642 is evidence that this GC has lost most of its low mass stars to the field. In order to quantify the slope of the observed PDMFs we carry out power-law fits to the curves shown in Fig. 7. The resulting slopes  $\alpha$  are shown in Table 1. Notice again the clear evidence for mass segregation, with a PDMF much more depleted of low-mass stars in the central regions.

We should point out that this inverted PDMF slope has been observed in other recent studies. Andreuzzi et al. (2001) found a power-law slope  $\alpha \simeq 0.9$  for NGC 6712 for masses  $m \leq 0.8M_\odot$  and argue that this GC is very vulnerable to tidal disruption. De Marchi & Pulone (2007) also find a PDMF with decreasing number of stars at lower masses ( $\alpha \simeq 0.5$ , in the range  $0.2 \leq m/M_\odot \leq 0.8$ ) in NGC 2298. Finally, Paust et al. (2009) obtain a PDMF that peaks near the MSTO in NGC 6366.

Simulations of GC (Baumgardt & Makino 2003) show that in tidal fields the preferential depletion of low-mass stars leads to a PDMF with inverted slope when the cluster has undergone 90% or more of its associated dissolution time. The time scale associated with the slope inversion phenomena is related to the time when the compact stellar remnants start to dominate the cluster mass. Since NGC 6642 is a very old GC that resides in a central region of the Galaxy the shape of the PDMF can easily be understood in the context of tidal interactions.

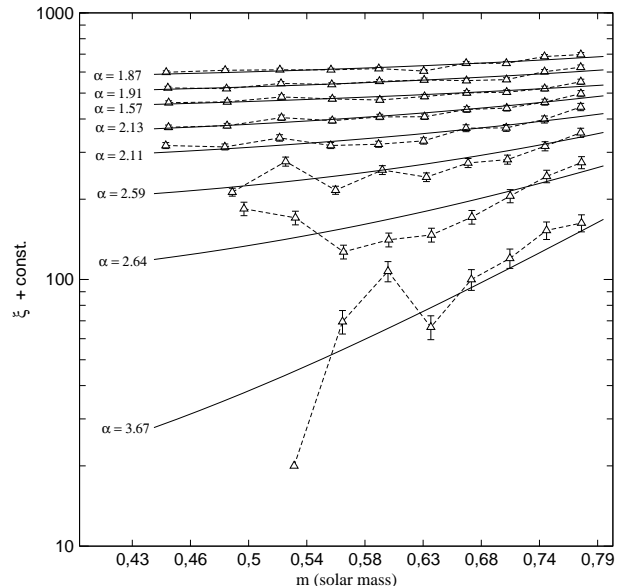


**Figure 7.** Present day mass functions (PDMFs) for different annuli around the centre of NGC 6642. Distance from cluster centre increases upwards. We use the same radial bins used for the LFs. A constant offset was added to the star counts to avoid confusion. Fits to a power-law PDMF are also shown and the corresponding slope values given. They are also listed in Table 1.

$\Delta r('')$	$m(M_\odot)$	$\alpha$
0 - 4.9	0.56 - 0.78	$3.67 \pm 0.93$
4.9 - 9.8	0.53 - 0.78	$2.64 \pm 0.88$
9.8 - 14.7	0.52 - 0.78	$2.59 \pm 0.60$
14.7 - 19.6	0.45 - 0.78	$2.11 \pm 0.41$
19.6 - 24.5	0.45 - 0.78	$2.13 \pm 0.21$
24.5 - 29.4	0.45 - 0.78	$1.57 \pm 0.23$
29.4 - 34.3	0.45 - 0.78	$1.91 \pm 0.26$
34.3 - 39.2	0.45 - 0.78	$1.87 \pm 0.36$

**Table 1.** Results of the power-law fitting to the MF at different radii. Column 1 lists the radial bin in arcseconds; column 2 gives the selected mass limits for the analysis; column 3 shows fitted slopes  $\alpha$ .

### 3.5 Horizontal Branch Morphology

We here determine the HB morphology using the parametrization described in Lee, Demarque & Zinn (1994)

$$HB_{index} = \frac{B - R}{(B + R + V)} \quad (4)$$

where B is the number of stars in the blue part of the HB, R is the number of stars in the red part and V is the number of variable stars. To determine the colour of the RR-Lyrae instability strip we used the HB analysis of the halo GC NGC 4147 by Stetson (2005). This cluster has a  $[Fe/H]$  very similar to NGC 6642. Stetson (2005) lists mean BVI magnitudes and colours for a sample of well known RR-Lyrae in NGC 4147. We used the full range of mean colours as the instability strip. Our photometry was converted to the standard system by means of the transformations from

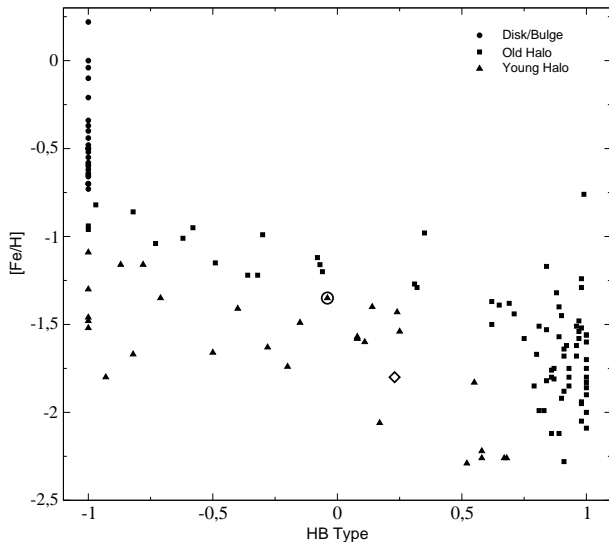


**Figure 8.**  $HB_{index}$  vs.  $[Fe/H]$  diagram from Mackey & Gilmore (2004). Here we show the Old Halo clusters (solid boxes), Young Halo clusters (solid triangles) and the Disk/Bulge clusters (solid circles). The solid triangle inside the open circle indicates the original position of NGC 6642 while the open diamond shows the position found in this work.

Sirianni et al. (2005). The resulting index is then  $HB_{index} \approx 0.25$ .

An alternative approach to determine  $HB_{index}$  is to use the colour range of the instability strip quoted by Mackey & Gilmore (2004), based on the work of Smith (1995) and on the data from Piotto et al. (2002). These limits are in  $(B - V)$  and were converted to  $(V - I)$  using colour-colour transformations from Caldwell et al. (1993). The result is then  $HB_{index} = 0.23$ . This is in close agreement with the previous estimate. We use the uncertainties of 0.02 mag in the stability strip limits quoted by Mackey & Gilmore (2004) and propagate them into  $HB_{index}$ . Our final result is then  $HB_{index} = 0.23^{+0.05}_{-0.01}$ . This value is in apparent disagreement with that calculated by Mackey & Gilmore (2004) for NGC 6642 using the same limits but applied to the published CMDs from Piotto et al. (2002):  $HB_{index} = -0.04 \pm 0.14$ . This discrepancy, however, is dominated by the different reddening corrections adopted. We use  $E(B - V) = 0.46$  whereas Piotto et al. (2002) find  $E(B - V) = 0.41$ . A lower  $E(B - V)$  systematically shifts the entire HB towards redder intrinsic colours. This certainly yields a lower index. If we adopt this smaller  $E(B - V)$  value to correct our observed HB and again apply the same colour range as Mackey & Gilmore (2004), we obtain  $HB_{index} = 0.05^{+0.07}_{-0.09}$ .

With  $HB_{index}$  at hand, we may plot NGC 6642 in the HB-type vs. metallicity diagram. Mackey & Gilmore (2004) use  $[Fe/H] = -1.35$  for NGC 6642 and place it as a member of the Young Halo subsystem, according to the classification of van den Bergh (1993). Our  $HB_{index}$  and  $[Fe/H]$  estimates confirm this position as far as the HB morphology is concerned, displacing NGC 6642 even further from the Old Halo and Disk/Bulge loci as seen in Fig. 8. On the other hand, its age and position in the Galaxy suggest that

NGC 6642 is more likely an inner halo than an outer bulge transition object.

## 4 DISCUSSION

We studied the GC NGC 6642 with ACS/HST imaging in the F606W and F814W bands using combined long and short exposures. The ACS/HST photometry employed here makes it possible to resolve stars well in the vicinity of the cluster's collapsed core.

From the GC CMD we have derived an age of  $13.8 \pm 1.6$  Gyr and  $[Fe/H] = -1.80 \pm 0.20$ . We also derived a colour excess of  $E(B - V) = 0.46 \pm 0.02$  towards NGC 6642 and a distance from the Sun comparable to that of the Galactic centre,  $d_{\odot} = 8.05 \pm 0.66$  kpc. Given the direction of NGC 6642 on the sky, and assuming that the distance from the Sun to the Galactic Centre is  $d_{C,\odot} = 8.0$  kpc, we conclude that NGC 6642 in fact currently occupies a very central position in the Galaxy,  $D_{C,clus} = 1.4$  kpc.

NGC 6642 has a very dense central core. Therefore, it is likely to be composed of stars that have undergone (or are undergoing) mergers. The very dense central object seen in Fig. 1 is not well resolved, although a high fraction of the BS are found in its vicinity. The radial density profile shows no evidence of a well resolved core, corroborating the idea that NGC 6642 is a core-collapsed GC.

A number of other surrounding BS candidates has been found. Their spatial distribution is more concentrated towards the GC centre than other GC stars, such as those in the HB. This result can also be interpreted in the context of the BS formation by merger scenario. We also observe a hint of bimodal radial density profile of the BS candidates, with a depletion region in the middle. These are common features in GCs (Dalessandro et al. 2008b).

The studied CMD also exhibits a well developed HB from which we could estimate  $HB_{index}$  as defined in Lee, Demarque & Zinn (1994). Along with the  $\log(\tau(\text{yrs}))$  and  $[Fe/H]$  values found in this work, our analysis shows that NGC 6642 is an unusual GC. It has an old age and a central location in the Galaxy, but its position in the  $[Fe/H]$  and  $HB_{index}$  plane is more consistent with the young halo GC system. Having in mind its atypical behaviour concerning its dynamical evolution and HB morphology, NGC 6642 is more likely to be a of a transition class between the inner halo and outer bulge cluster population.

The analysis of the LF and PDMF and their variation as a function of radius shows a clear evidence for mass segregation, especially in the range  $0.4 \leq m/m_{\odot} \leq 0.8$ . Furthermore, in all regions, there is a decrease in the star counts towards lower luminosities and masses, an effect which is stronger in the central regions. This inversion in the PDMF slope is atypical, although it has been previously observed and is supported by dynamical N-body simulations (Andreuzzi et al. 2001; De Marchi & Pulone 2007; Paust et al. 2009). Our findings concerning the PDMF of NGC 6642, which resides in a violent environment, can be explained in terms of disk and bulge shocking through its perigalacticon passages (Baumgardt & Makino 2003). The high resolution images available nowadays are allowing us to observe these phenomena more frequently and strongly

suggest that dynamical effects over a GC life-time have a dominant contribution from the external environment.

An interesting feature that is expected to result from the high degree of depletion of low mass stars is the presence of a tidal tail around NGC 6642. For this purpose, a more sophisticated field decontamination technique must be adopted such as the statistical analysis of CMDs (Kerber et al. 2002). From the analysis of the RDP of NGC 6642 it is not clear that we have reached the tidal radius of the GC; thus, for the analysis of a possible tidal tail it is necessary to have images with a wider field. The tidal tail search could make the estimate of the mass loss due to tidal erosion possible.

**Acknowledgments.** This work was supported by Conselho Nacional de Desenvolvimento Científico e Tecnológico (CNPq) in Brazil.

## REFERENCES

- Aguilar L., Hut P., & Ostriker J., 1988, *ApJ*, 335, 720  
 Andreuzzi G., De Marchi G., Ferraro F., Paresce F., Pulone L., & Buonanno R., 2001, *A&A*, 372, 851  
 Baraffe I., Chabrier G., Allard F., Hauschildt P. H., 1998, *A&A*, 337, 403  
 Barbuy, B., Bica, E., Ortolani, S. & Bonatto, C., 2006, *A&A*, 449, 1019  
 Baumgardt H., & Makino J., 2003, *MNRAS*, 340, 227  
 Bellazzini M., 2007, *A&A*, 473, 171  
 Caldwell J., Cousins A., Ahlers C., van Wamelen P., & Maritz E., 1993, *SAAO Circulars*, n. 15.  
 Dalessandro E., Lanzoni B., Ferraro F., Vespe F., Bellazzini M., & Rood T., 2008, *ApJ*, 681, 311  
 Dalessandro E., Lanzoni B., Ferraro F., Rood T., Milone A., Piotto G., Valenti E., & 2008, *ApJ*, 677, 1069  
 De Marchi G., & Pulone L., 2007, *A&A*, 467, 107  
 Dolphin A. E., 2000, *PASP*, 112, 1383  
 Ferraro F., Sollima A., Rood R., Origlia L., Pancino E., & Bellazzini M., 2006, *ApJ*, 638, 433  
 Glatt K., Gallagher J., Grebel E., et al, 2008, *AJ*, 135, 1106  
 Girardi L., Bressan A., Bertelli G., & Chiosi C., 2000, *A&AS*, 141, 371  
 Harris W.E., 1996, *AJ*, 112, 1487  
 Ivanov V., Kurtev R., & Borissova J., 2005, *A&A*, 442, 195  
 Kerber L., Santiago B., Castro, R. & Valls-Gabaud, D., *A&A*, 390, 121  
 Lee Y. -W., Demarque P. & Zinn R., 1994, *ApJ*, 423, 248  
 Mackey A. D. & Gilmore G. F., 2004, *MNRAS*, 355, 504  
 Minniti D., 1995, *A&A*, 303, 468  
 Marin-Franch A., Aparicio A., Piotto G. et al. 2009, arXiv0812.4541  
 Norris J., Freeman K. & Mighell K. 1996, *ApJ*, 462, 241  
 Paust N., Aparicio A., Piotto G., et al., 2009, *AJ*, 137, 246.  
 Origlia L., Valenti E., Rich R. & Ferraro F., 2005, *MNRAS*, 363, 897  
 Ortolani S., Bica E. & Barbuy B., 2006, *ApJ Letters*, 646, L115  
 Piotto G., King I., Djorgovski S., Sosin C., Zoccali M., Saviane I., De Angeli F et al., 2002, *A&A*, 391, 945  
 Richer H., Dotter A., Hurley J., et al., *AJ*, 135, 2141  
 Sarajedini, A., Bedin, L., Chaboyer, B., et al., *AJ*, 133, 1658  
 Shin J., Kim S., & Takahashi K., 2008, *MNRAS*, 386, L67  
 Sirianni M., Jee M., Benítez N., Blacklee J., Martel A., Meurer G., et al. 2005, *PASP*, 117, 1049  
 Smith H., 1995, *RR Lyrae stars*, Cambridge University Press, Cambridge  
 Sollima A., Ferraro F., Pancino E., Bellazzini M., 2005, *MNRAS*, 357, 265  
 Stetson P. B., 2005, *PASP*, 117, 1325  
 Trager S.C., King Ivan. R., Djorgovski S., 1995, *AJ*, 109, 218  
 van den Bergh S., 1993, *ApJ*, 411, 178  
 Walker A., 1992, *ApJ*, 390, L81